

Low-power electro–optic phase modulator based on multilayer graphene/silicon nitride waveguide*

Lanting Ji(姬兰婷)^{1,2}, Wei Chen(陈威)¹, Yang Gao(高阳)¹, Yan Xu(许言)¹, Chi Wu(吴轶)², Xibin Wang(王希斌)¹, Yunji Yi(衣云骥)¹, Baohua Li(李宝华)¹, Xiaoqiang Sun(孙小强)^{1,†}, and Daming Zhang(张大明)¹

¹State Key Laboratory of Integrated Optoelectronics, College of Electronic Science & Engineering, Jilin University, Changchun 130012, China

²Institute of Marine Science and Technology, Shandong University, Qingdao 250100, China

(Received 13 February 2020; revised manuscript received 2 April 2020; accepted manuscript online 19 May 2020)

Electro–optic modulator is a key component for on-chip optical signal processing. An electro–optic phase modulator based on multilayer graphene embedded in silicon nitride waveguide is demonstrated to fulfill low-power operation. Finite element method is adopted to investigate the interaction enhancement between the graphene flake and the optical mode. The impact of multilayer graphene on the performance of phase modulator is studied comprehensively. Simulation results show that the modulation efficiency improves with the increment of graphene layer number, as well as the modulation length. The 3-dB bandwidth of around 48 GHz is independent of graphene layer number and length. Compared to modulator with two- or four-layer graphene, the six-layer graphene/silicon nitride waveguide modulator can realize π phase shift at a low-power consumption of 14 fJ/bit when the modulation length is 240 μm .

Keywords: electro–optic modulator, graphene, silicon nitride, waveguide

PACS: 42.79.Hp, 42.79.Gn, 78.67.Wj

DOI: 10.1088/1674-1056/ab943b

1. Introduction

Electro–optic (EO) modulators are key components to generate or modulate high speed optical signals in a photonic integrated system. EO modulators based on different approaches have been reported. Commercially available lithium niobate-based EO modulators are technically mature, however, suffering from large size and relatively high drive voltage.^[1] The plasma dispersion effect-based silicon modulator is CMOS-compatible. Unfortunately, the accompanied chirp and limited EO coefficient deteriorates its performance.^[2] Franz-Keldysh effect-based Ge or SiGe electro-absorption (EA) modulator is with wide bandwidth and easy integration, except that the thermal stability and insertion loss are supposed to be improved.^[3] The hybrid plasmonic waveguide modulator based on nonlinear polymer is compact and low-power consumption. The challenge is the long-term working stability and compatibility with CMOS technology.^[4]

By contrast, graphene, a two-dimensional (2D) mono-atomic material, has favorable optical properties of high conductivity, high modulation efficiency, wide bandwidth, and tunable optical absorption.^[5–11] The complex permittivity of graphene can be tuned by actively tuning the Fermi level through applying the drive voltage. However, the single atomic thick graphene has weak interaction to the vertical incident light (only $\sim 2.3\%$ absorption), which limits its applica-

tion in EO modulators.^[12–15] The hybrid integrated waveguide structure can increase the density of electric field in graphene layer, which leads to the improvement of reciprocal reaction between the optical mode and graphene flake. Therefore, graphene-based silicon-on-insulator (SOI) hybrid integrated waveguide EO modulators have been widely studied.^[16–28] However, due to the surface roughness of silicon stripe, the propagation loss of SOI waveguide is relatively large (about 2 dB/cm to 3 dB/cm).^[29] Comparatively, silicon nitride (SiN) waveguides has much lower propagation loss of ~ 0.1 dB/cm. The refractive index difference between the SiN core and silica cladding is smaller compared to that in SOI waveguide, which leads to the relatively larger single-mode field dimension and resulted loss reduction for end-face coupling.^[30–32] Different graphene-based SiN waveguide modulators have been proposed,^[29,33,34] most of which are based on the tunable electro-absorption of graphene. While, graphene induced electro-refraction effect is intrinsically fit for phase modulation. Though electro-refractive phase modulation in graphene has been reported,^[17,19,23,26,35,36] the waveguide configuration is still deserved to be investigated for better performance, such as reducing the capacitance and gate voltage, as well as optimizing the bandwidth and power consumption under conservative values.

In this paper, a multilayer graphene-based SiN waveguide (GSNW) phase modulator is demonstrated. The impact of

*Project supported by the National Key Research and Development Program of China (Grant No. 2019YFB2203001), the National Natural Science Foundation of China (Grant Nos. 61675087, 61875069, and 61605057), and the Science and Technology Development Plan of Jilin Province, China (Grant No. JJKH20190118KJ).

†Corresponding author. E-mail: sunxq@jlu.edu.cn

graphene layers and modulation length on the performance of phase modulation are investigated by finite element method. The results show that quasi-linear phase change can be realized by the electro-refraction effect of graphene. The drive voltage V_π (for a π phase shift) decreases with the increment of graphene layer number, as well as the modulation length. The 240- μm -long six-layer GSNW phase modulator demands a minimum power consumption of 14 fJ/bit to realize a π phase shift. The 3-dB bandwidth ($f_{3\text{ dB}}$) is around 48 GHz for all conditions. A balanced performance can be expected based on the proposed design rule.

2. Configuration and principle

The designed phase modulator is schematically shown in Figs. 1(a) and 1(b). Two graphene layers are embedded in the SiN ($n_{\text{SiN}} = 1.98$) waveguide to enhance the light-graphene interaction. Silica ($n_{\text{silica}} = 1.44$) is selected as the cladding material. The palladium-graphene ohmic contacts are formed by depositing metal palladium onto the graphene flakes to extract the electrodes.^[37] A capacitance structure is formed by the two separated graphene sheets with 10-nm-thick hexagonal boron nitride (hBN) insulator layer ($n_{\text{hBN}} = 1.98$). Considering the challenge in alignment, the lower SiN waveguide is embedded in silica substrate. Here, the height and width of SiN waveguide are denoted by h_{SiN} and w_{SiN} , respectively. L_g and w_g correspond to the length and effective width of graphene, w_{ol} refers to the common width between two graphene layers.

The single atomic 2D plane graphene exhibits characteristic of anisotropy. Its in-plane permittivity may be adjusted by Fermi level μ_c .^[38,39] Figure 2 shows the in-plane permittivity as a function of μ_c at the wavelength 1550 nm.^[28] Both the real and imaginary parts vary remarkably as μ_c increases from 0.35 eV to 0.45 eV. When μ_c is lower than 0.38 eV, the real part of permittivity $\text{Re}(\epsilon_{\parallel})$ varies inversely with μ_c . Differently, $\text{Re}(\epsilon_{\parallel})$ quasi-linearly reduces as μ_c is larger than 0.4 eV. When μ_c shifts from 0.35 eV to 0.45 eV, the imaginary part $\text{Im}(\epsilon_{\parallel})$ decreases rapidly. When μ_c is smaller than 0.35 eV, the interband transition of graphene dominates and the photon absorption is relatively strong. If μ_c is larger than 0.5 eV, the interband transition of graphene electrons become saturate and the intraband transition dominates. It can be seen that the photon absorption of graphene keeps at a low level supposing μ_c is tuned to block the interband transitions. As a result, only the mode phase is quasi-linearly changed, while the amplitude almost keeps static.

The variation of applied driving gate voltage results in the changing of μ_c , as well as the complex permittivity of graphene (ϵ_{\parallel}). Accordingly, the effective mode index (EMI) of GSNW may be adjusted by tuning ϵ_{\parallel} . Since the real part and imaginary part of EMI determine the electro-refraction and

electro-absorption of graphene, respectively, the phase change and power attenuation of mode propagating in GSNW can be implemented by applying external voltage.^[17,18] The relationship between phase change $\Delta\phi$ and the real part of EMI variation $\Delta\text{Re}(N_{\text{eff}})$ can be written as

$$\Delta\phi = \frac{2\pi}{\lambda} \Delta\text{Re}(N_{\text{eff}}) L_g, \quad (1)$$

where λ is the operation optical wavelength in vacuum. The maximization of $\text{Re}(N_{\text{eff}})$ leads to better phase modulation performance. Correspondingly, the mode propagation attenuation (MPA) can be estimated as

$$\text{MPA} = \frac{40\pi(\log_{10} e)\text{Im}(N_{\text{eff}})}{\lambda}, \quad (2)$$

where $\text{Im}(N_{\text{eff}})$ is the imaginary part of the EMI. As shown in Fig. 2, a larger $\Delta\text{Re}(N_{\text{eff}})$ commonly accompanies with a higher $\text{Im}(\epsilon_{\parallel})$ or loss. The phase modulation efficiency is in conflict with the optical loss. Therefore, compromise parameters combination is demanded in the design process.

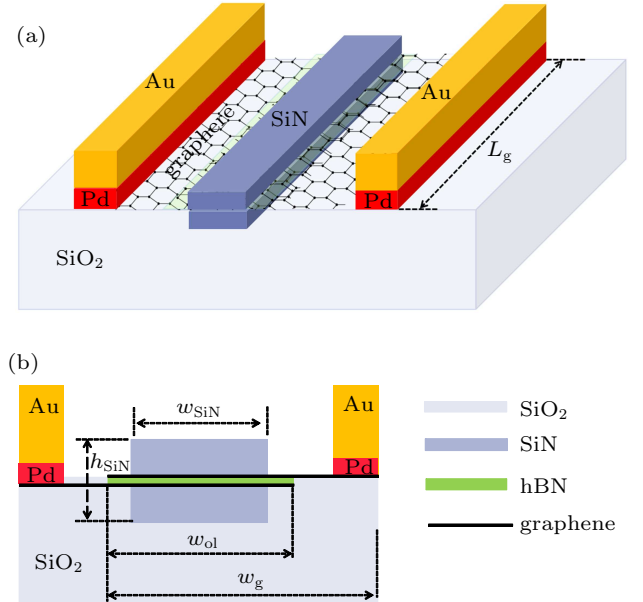


Fig. 1. (a) Three-dimensional (3D) and (b) cross-sectional view of the graphene-based Si₃N₄ waveguide electro-optic modulator.

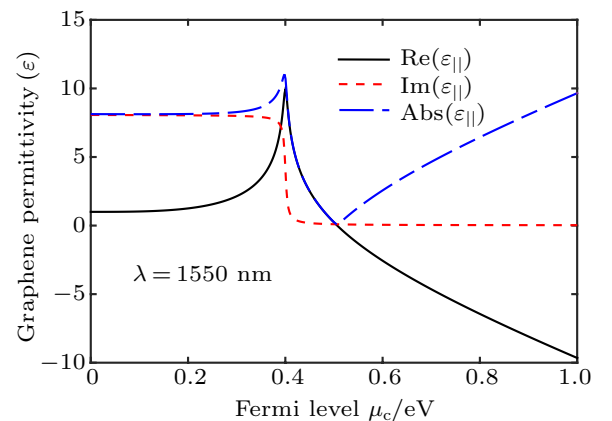


Fig. 2. In-plane permittivity changes with Fermi level μ_c of graphene at 1550 nm.

3. Design and optimization

3.1. SiN waveguide

Since graphene has more remarkable impact on the EMI of TE mode compared with that on the EMI of TM mode, we then investigate the EMI of fundamental TE mode. For graphene-based waveguide modulators, light absorption at the neutral point is a measurement of interaction strength between the waveguide optical mode and the graphene layer. As shown in Fig. 3, $\text{Im}(N_{\text{eff}})$ that changes with the SiN waveguide height h_{SiN} and width w_{SiN} is firstly calculated by finite-element method as μ_c is 0 eV. When $w_{\text{SiN}} > 800$ nm and $h_{\text{SiN}} < 400$ nm, $\text{Im}(N_{\text{eff}})$ that corresponds to the optical absorption is relatively large. This mainly attributes to the fact that a wider waveguide gives rise to a longer interaction length between the electric field component in x direction and the graphene layer, resulting in a larger optical extinction coefficient. When the height of SiN waveguide h_{SiN} is decreasing, the electric field energy density in the waveguide is increasing, leading to an enhancement of reciprocal action between the optical mode and graphene flakes. As a result, the $\text{Im}(N_{\text{eff}})$ increases with the decrease of h_{SiN} . The width and thickness of waveguide are accordingly chosen to be 850 nm and 360 nm, respectively. Though smaller waveguide dimension implies larger $\text{Re}(N_{\text{eff}})$ change, however, it is more close to cut-off, and leading to higher loss.

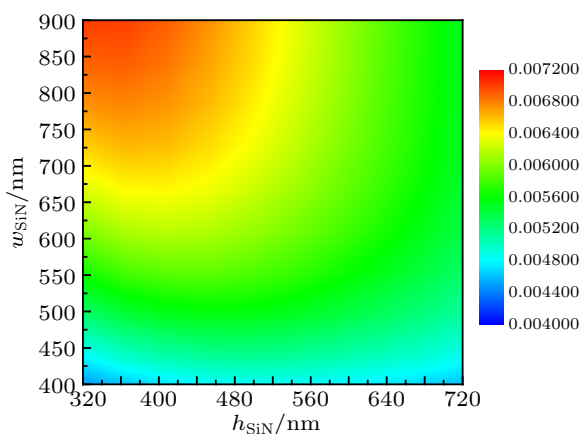


Fig. 3. $\text{Im}(N_{\text{eff}})$ of SiN waveguide as a function of h_{SiN} and w_{SiN} when μ_c is 0 eV ($\lambda = 1550$ nm).

3.2. Effect of graphene layers

Compared to single-layer graphene, multilayer graphene configuration has advantages of larger modulation depth, faster operation speed, and lower power consumption.^[13,18,20,35] For multilayer graphene waveguide structures, the effect of graphene layer number on the optical and the modulating performance is yet to be confirmed. We firstly investigate the mode field distributions of SiN waveguide with different layer numbers of graphene when w_{SiN} and

h_{SiN} are 850 nm and 360 nm, respectively. Figures 4(a), 4(c), and 4(e) show the cross-sectional view GSNW with two-, four-, and six-layer graphene configurations. Corresponding field distributions have been shown in Figs. 4(b), 4(d), and 4(f), respectively. It can be seen that the mode field is well confined within the waveguide in each case.

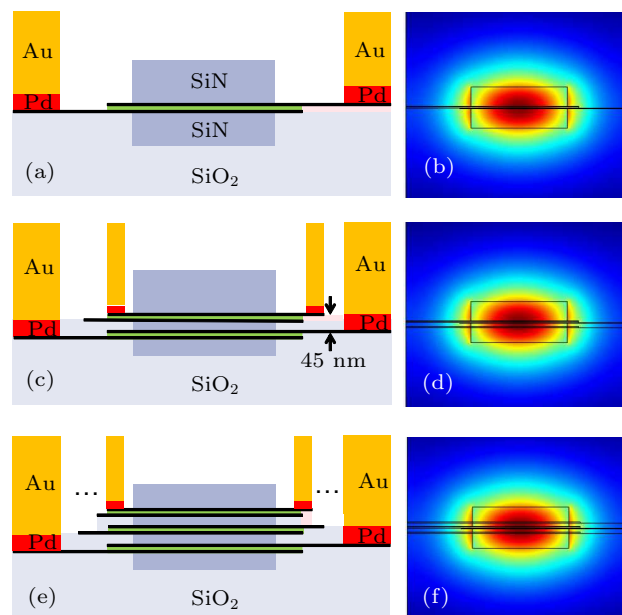


Fig. 4. Cross-section of (a) two-layer, (c) four-layer, and (e) six-layer GSNW configurations. Panels (b), (d), and (f) show field distributions of panels (a), (c), and (e), respectively.

Similarly, the EMI of fundamental TE mode as a function of μ_c for these two-, four-, and six-layer graphene configurations has been calculated and compared to study the impact of graphene layer number increment. As shown in Fig. 5(a), $\text{Re}(N_{\text{eff}})$ increases when μ_c varies from 0 eV to 0.38 eV. All ERIs declines quasi-linearly as μ_c increases from 0.45 eV to 1 eV. The largest $\text{Re}(N_{\text{eff}})$ change for the six-layer GSNW is almost 0.05, which is much higher than that in conventional EO materials of about 10^{-4} .^[17,40] Figure 5(b) shows the corresponding imaginary part $\text{Im}(N_{\text{eff}})$ for different layer numbers of graphene. $\text{Im}(N_{\text{eff}})$ reduces rapidly when μ_c varies from 0.35 eV to 0.45 eV, then keeps at a low level when μ_c is larger than 0.45 eV. When $\mu_c = 0$ eV, the maximum $\text{Im}(N_{\text{eff}})$ for the two-, four-, and six-layer graphene waveguides is 0.0069, 0.0136, and 0.0202, respectively. To be mentioned, the minimum values are very close for different graphene layer numbers at $\mu_c = 1$ eV. A larger number of graphene layers may impose more remarkable effect on the waveguide optical mode, leading to a higher modulation efficiency. For the sake of larger phase modulation and low-power operation, the insertion loss may be sacrificed as 6-layer graphene structure is adopted.

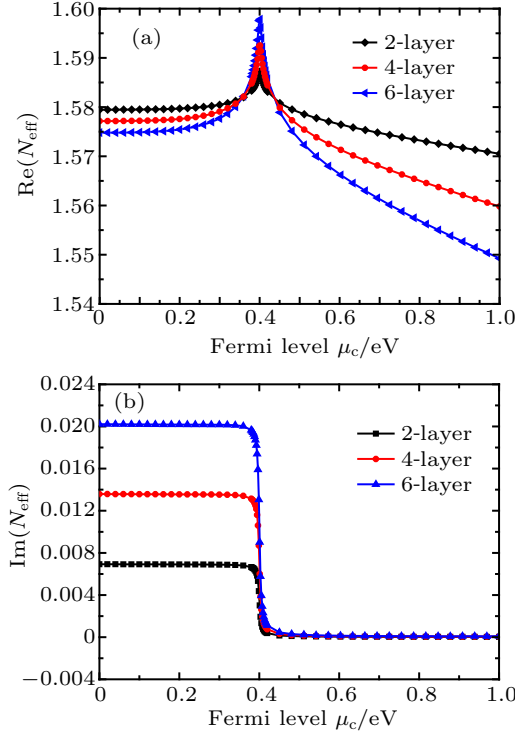


Fig. 5. (a) Real and (b) imaginary parts of N_{eff} as a function of Fermi level for different graphene layers.

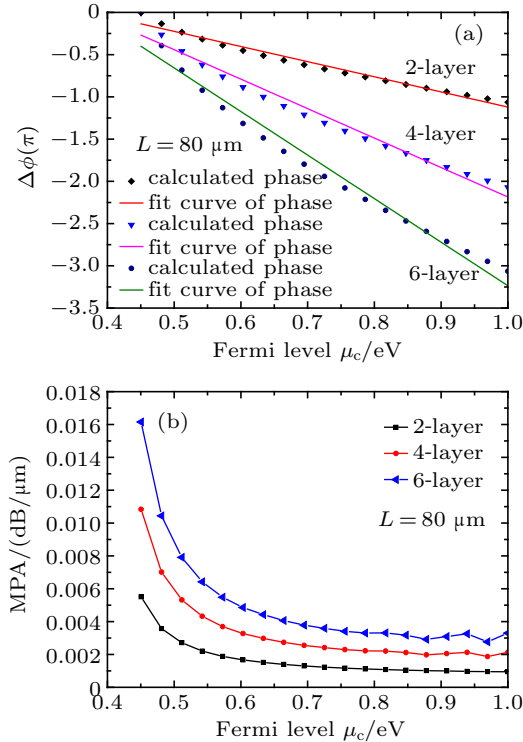


Fig. 6. Illustration of (a) quasi-linear variation of the optical phase, and (b) optical MPA versus Fermi levels for different numbers of graphene layer.

As the calculation presented in Fig. 5(a), when Fermi level μ_c is over 0.45 eV, $\text{Re}(N_{\text{eff}})$ decreases approximately linearly as the Fermi level increases, while the optical absorption stays at a low level. This favorable characteristic is beneficial to the optical phase modulation. Figure 6(a) illustrates the quasi-linear variation of the optical phase versus Fermi levels

for different graphene layers. In the simulation, the modulating length L_g is chosen to be 80 μm , and the phase shift at $\mu_c = 0.45$ eV is assumed to be zero. As shown in the figure, the quasi-linear phase shift of 0 to $-\pi$, 0 to -2π , and 0 to -3π may be implemented through shifting μ_c from 0.45 eV to 1 eV for the adoption of two-, four-, and six-layer numbers of graphene, respectively. In the meantime, the MPA decreases slightly when μ_c increases from 0.45 eV to 1 eV, as shown in Fig. 6(b). The light absorption of ~ 0.001 dB/ μm , ~ 0.002 dB/ μm , and ~ 0.003 dB/ μm for different graphene layers at $\mu_c = 1$ eV can be observed. The absorption for six-layer graphene is almost three times larger than that of two-layer graphene. The number increment of graphene can significantly enhance the modulation efficiency, meanwhile, increasing the optical loss.

The relationship between the applied gate voltage and Fermi level μ_c of graphene is estimated as

$$|\mu_c| = \hbar v_F \sqrt{\pi \eta |V_g - V_0|}, \quad (3)$$

where $v_F = 2.5 \times 10^6$ m/s is the Fermi velocity of graphene, η can be generated from $\epsilon_r \epsilon_0 / d_1 e$, where ϵ_r represents the permittivity of hBN, and $d_1 = 10$ nm is the vertical separation distance between two graphene flakes.^[42–44] For simplicity, $|V_g - V_0|$ as a whole is regarded as the applied driving voltage V . When this waveguide is implemented on one arm of Mach-Zehnder interferometer (MZI), the modulating arm length L is selected to be 80 μm . In the static state, the chemical potential on both two arms can set to be $\mu_{c1} = \mu_{c2} = 0.45$ eV to keep the phase balance. The corresponding gate voltage or bias voltage that is applied on the graphene sheets through Pd electrodes is 1.08 V. In the dynamic state, as the gate voltage of one arm rises, the phase shift leads to a variation of the transmission $T(\Delta\phi)$, which can be expressed as

$$T(\Delta\phi) = \frac{1}{4} \times \left[e^{-\text{Im}(\beta_1)L} + e^{-\text{Im}(\beta_2)L} + 2 \exp \left[-\frac{e^{-\text{Im}(\beta_1)L} + e^{-\text{Im}(\beta_2)L}}{2} \right] \cos(\Delta\phi) \right], \quad (4)$$

where $\beta_1 = 2\pi N_{\text{eff}1} / \lambda$ and $\beta_2 = 2\pi N_{\text{eff}2} / \lambda$ represent the propagation constants of two arms, respectively.^[45] The calculated results are shown in Fig. 7. For cases of two-, four-, and six-layer graphene structures to obtain the same π phase difference between these two arms, the driving voltage V_π is required to be 4.68 V, 2.15 V, and 1.56 V, respectively. At the bias voltage of 1.08 V, the corresponding insertion losses are around 0.22 dB, 0.43 dB, and 0.64 dB, respectively. The six-layer graphene-based waveguide has the largest loss of all but the minimum V_π . We believe this rule of loss increment is applicable to similar multilayer graphene-based waveguide structures.

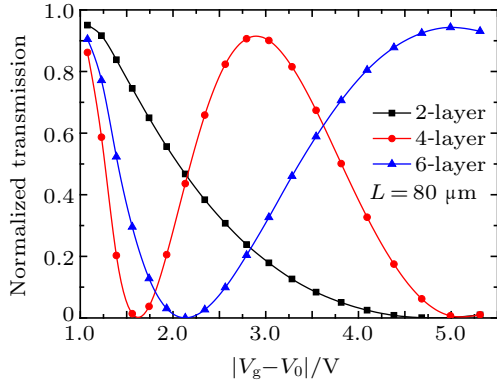


Fig. 7. Optical transmission of the MZI modulator changes with applied gate voltages for the 80- μm -long graphene with different layers.

3.3. Effect of modulating length

As has been reported, the modulating length has significant impact on the performance of a modulator. For simplicity, we only study the effect of two-layer graphene structure. The parameters change in the four- and six-layer graphene structures is supposed to exhibit similar behaviors. As shown in Fig. 8(a), the variation of phase shift as a function of μ_c at different modulating lengths of 80, 160, and 240 μm has been investigated, respectively. When μ_c shifts from 0.45 eV to 1 eV, $\Delta\phi$ can be quasi-linearly adjusted from 0 to $-\pi$, -2π , and -3.2π , respectively. When L_g is 240 μm , the phase tuning efficiency is over three times than the efficiency when L_g is 80 μm . As shown in Fig. 8(b), the optical loss firstly reduces quickly when μ_c increases from 0.45 eV to 0.6 eV. Then it gradually becomes saturated and gets stable when μ_c is larger than 0.6 eV. As shown in Fig. 8(b), for the 80-, 160-, and 240- μm -long graphene existences, the insertion losses of ~ 0.076 , ~ 0.152 , and ~ 0.228 dB at $\mu_c = 1$ eV can be observed, respectively. It is clear that a longer graphene length can enhance the modulation efficiency in the price of insertion loss, because the modulation length increment implies the stronger interaction between the graphene layer and optical field.

To specify the graphene length, the optical transmission of MZI modulator changing with the applied gate voltage at different L_g is investigated and shown in Fig. 9. To obtain the same π phase difference between two arms of MZI, the required gate voltages for the 80-, 160-, and 240- μm -long graphene structures are 4.68, 2.10, and 1.57 V, respectively. For lower voltage operation, the modulating graphene length is deserved to be 240 μm .

To be noted, the impact of both the graphene layer number and the modulation length on the performance of phase modulator are studied in Figs. 6(a) and 8(a), respectively. The difference between Figs. 6(a) and 8(a) is the precondition. In Fig. 6(a), the graphene length is fixed at 80 μm . The phase change is investigated as a function of Fermi level for dif-

ferent graphene layer numbers. Differently, in Fig. 8(a), the graphene layer number is fixed at 2-layer. The phase change is studied as a function of Fermi level for different graphene lengths. Therefore, the phase changes $\Delta\phi$ as a function of Fermi level for a 80- μm -long, 2-layer GSNW are the same in Figs. 6(a) and 8(a). However, different rules have been uncovered by Figs. 6(a) and 8(a). From Fig. 6(a), it can be seen that the graphene layer number increment can enhance the phase modulation efficiency. From Fig. 8(a), it is revealed that the graphene length increment also can improve the phase modulation efficiency. However, both are in the price of optical loss. Therefore, similar trends can be observed in Figs. 6(a) and 8(a).

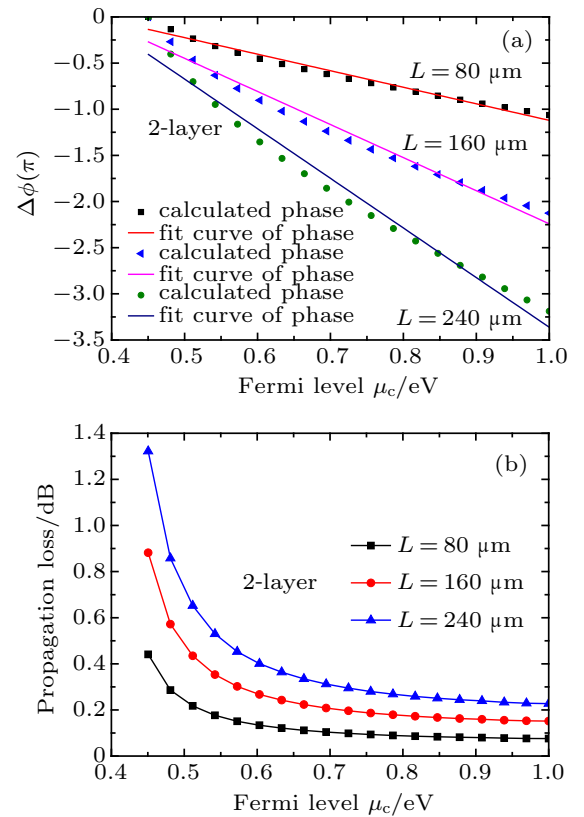


Fig. 8. Illustration of (a) quasi-linear variation of the optical phase, and (b) insertion loss *versus* Fermi levels for different graphene modulation lengths.

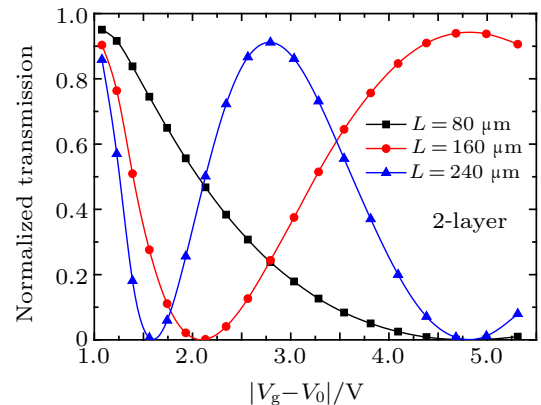


Fig. 9. Normalized transmission of the MZI modulator changes with applied gate voltage for the two-layer graphene at different modulating lengths.

4. Performance and discussion

In practical applications, the bandwidth and power consumption of modulator closely relate to the effective resistance and capacitance. Therefore, multilayer graphene phase modulators are investigated by the equivalent electrical circuit model, as shown in Fig. 10.

Taking the two-layer graphene modulator as an example, as shown in Fig. 10(a), the capacitance formed by two parallel graphene sheets and hBN insulator consists of the dielectric capacitance C_{ox} and the quantum capacitance C_Q . The consideration of series capacitance will lead to the decrement of total capacitance and resulted faster speed. To simplify the calculations, the quantum capacitance C_Q has been omitted here. Based on parallel plate capacitance model, the dielectric capacitance C_{ox} can be expressed as

$$C_{ox} = \epsilon_r \epsilon_0 w_{ol} L_g / d_1, \quad (5)$$

where ϵ_r is the dielectric constant of hBN, the overlap width w_{ol} between the upper and lower graphene is 1.1 μm . The vertical separation distance of the two graphene flakes d_1 is 10 nm. Then, C_{ox} is calculated to be 30 pF.

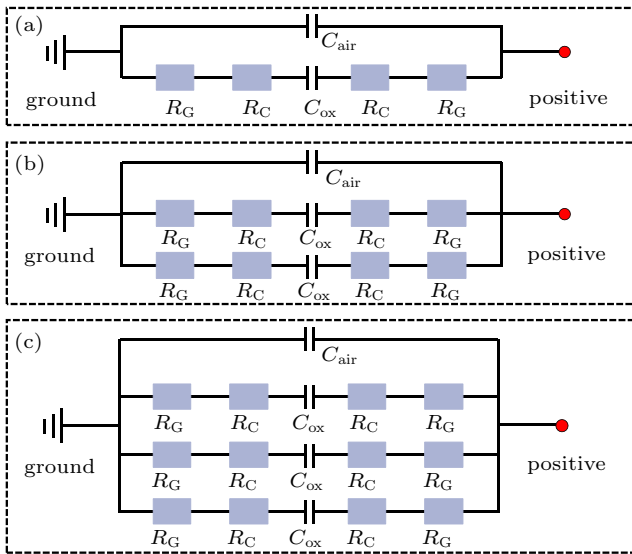


Fig. 10. Equivalent electrical circuits of (a) two-, (b) four-, and (c) six-layer graphene modulators.

The effective resistance R , which is composed of the sheet resistance R_G and the P_d /graphene contact resistance R_C , can be described as^[13,46]

$$R = 2R_G \times \frac{w_g}{L} + \frac{2R_C}{L}, \quad (6)$$

where the effective width of graphene sheet w_g is 1.6 μm . R_G may be tuned from 100 Ω/\square to 300 Ω/\square , which corresponds to a mobility from 6900 $\text{cm}^2/\text{V}\cdot\text{s}$ to 2300 $\text{cm}^2/\text{V}\cdot\text{s}$. Compromisingly, R_G is chosen to be 200 Ω/\square ,^[30] while R_C is selected to be 100 $\Omega \cdot \mu\text{m}$ ^[41] in calculations.

Theoretically, RC delay will play a main role in the determination of bandwidth $f_{3\text{ dB}}$. Based on the proposed electric circuit model, $f_{3\text{ dB}}$ can be evaluated by

$$f_{3\text{ dB}} = \frac{1}{2\pi R_{\text{total}} C_{\text{total}}}, \quad (7)$$

where C_{total} is the circuit total capacitance that includes C_{air} and C_{ox} , R_{total} is the circuit total resistance.^[47] R_{total} is R , $R/2$, and $R/3$ for two-, four-, and six-layer graphene structures, respectively. C_{total} is $C_{\text{air}} + C_{\text{ox}}$, $C_{\text{air}} + 2C_{\text{ox}}$, and $C_{\text{air}} + 3C_{\text{ox}}$ for two-, four-, and six-layer graphene structures, respectively. The average power consumption is evaluated by energy per bit, and it may be expressed as

$$E_{\text{bit}} = C_{\text{total}} (\Delta U^2 / 4), \quad (8)$$

where ΔU is the difference between the driving voltage and bias voltage. For four- and six-layer graphene phase modulator performance evaluations, above equations can work, too.

In this work, the MZI structure adopting the multilayer graphene/SiN waveguide in two separate arms is used to reveal the phase modulating performance. A summary of calculations is illustrated in Table 1. It can be seen that $f_{3\text{ dB}}$ is around 48 GHz for all conditions, because the product of $R_{\text{total}} \times C_{\text{total}}$ show unremarkable change in different graphene layer conditions. For six-layer graphene modulators, when L_g is 240 μm , the minimum driving voltage demand of 0.14 V, the smallest power consumption of 0.014 fJ/bit, and the largest insertion loss of 1.92 dB can be observed. Similarly, for two-layer graphene modulators, when L_g is 240 μm , the minimum driving voltage of 0.49 V, a smallest power consumption of 0.057 fJ/bit, and the maximum insertion loss of 0.66 dB can be observed, compared with performances of the 80- μm or 160- μm -long two-layer graphene modulators. Obviously, graphene layer number plays a key role in the determination of power consumption and optical loss for modulators with the same graphene length. The conflict between power consumption and optical loss implies the practical modulator parameters are supposed to be determined on the primary requirement. If low-power consumption or wider bandwidth is the main issue, the six-layer GSNW modulator is more preferable. If loss property is the critical issue, the two-layer graphene/SiN waveguide would provide better performance. Consideration from different aspects leads to different design preferences.

Another challenge for proposed multilayer GSNW phase modulator is the fabrication. The two-layer graphene modulator is supposed to be implemented on a silica substrate. The 850-nm-wide and 360-nm-high SiN waveguide surrounded by silica can be fabricated by using standard technologies, including chemical vapor deposition (CVD), electron-beam lithography (EBL), plasma etching.^[48,49] The even surface above the

SiN waveguide can be formed by silicon oxide deposition with plasma-enhanced chemical vapor deposition (PECVD) technique, and sequential chemical–mechanical polishing (CMP). The most challenging part may be the formation of stacked graphene/hBN heterostructures with high quantity on the SiN waveguide. According to reported works, CVD and wet-transferring could form the first graphene flake on the top SiN waveguide.^[50–52] The UV photo lithography and followed oxygen plasma etching are supposed to define the graphene-covered SiN waveguide region. Metal contacts can be formed by another UV lithography, Au/Pd metal deposition and lift-off process. After the deposition of 10-nm-thick hBN on the first graphene flake, the second graphene flake can be wet-transferred, too. Followed photo lithography and oxygen plasma etching will define the overlap region. The four-layer

and six-layer stacked graphene/hBN heterostructures can be constructed by the same method. The top SiN waveguide may be formed by the same process discussed above.

To convincingly illustrate the characteristics of proposed design, key parameters of the multilayer GSNW phase modulator are compared with those of reported theoretical works. As shown in Table 2, the 80- μm -long, 2-layer GSNW modulator proposed in this work has the lowest insertion loss of 0.22 dB. The 80- μm -long 6-layer GSNW modulator exhibits the smallest power consumption of 0.054 pJ/bit. Besides, the proposed multilayer GSNW design shows balanced performance of footprint and bandwidth. Therefore, we believe this GSNW phase modulator design has good potentials in practical applications.

Table 1. Modulating performance of different GSNW modulators.

Structure Layer number	MZI								
	2			4			6		
$L_g/\mu\text{m}$	80	160	240	80	160	240	80	160	240
$C_{\text{total}}/\text{pF}$	0.322	0.632	0.942	0.632	1.252	1.872	0.942	1.872	2.802
R_{total}/Ω	10.5	5.25	3.50	5.25	2.63	1.75	3.50	1.75	1.17
$\Delta U/V$	3.60	1.02	0.49	1.07	0.34	0.20	0.48	0.19	0.14
Power/(pJ/bit)	1.043	0.164	0.057	0.181	0.036	0.019	0.054	0.017	0.014
f_3 dB/GHz	47.1	48.0	48.3	48.0	48.5	48.6	48.3	48.6	48.6
IL/dB	0.22	0.44	0.66	0.43	0.86	1.29	0.64	1.28	1.92

Table 2. Performance comparison between graphene-based phase modulators.

Description	Length/ μm	f_3 dB/GHz	Power/(pJ/bit)	Bias/V	Insertion loss/dB
Graphene on Si WG ^[17]	75.6	119.5	0.452	1	1.37
Graphene-Si on slot WG ^[24]	100	500	NA	1.3	0.97
2-layer graphene in SOI ^[35]	500	30	0.38	7.8	0.6
1-layer graphene in SOI ^[35]	850	19	0.66	6.5	2.805
Graphene on ultrathin Si WG ^[36]	96.63	14.2	0.097	3.87	1.55
This work (2-layer GSNW)	80	47.1	1.043	1.08	0.22
This work (4-layer GSNW)	80	48.0	0.181	1.08	0.43
This work (6-layer GSNW)	80	48.3	0.054	1.08	0.64

5. Conclusion and perspectives

A multilayer GSNW electro–optic phase modulator has been theoretically investigated. The effect of graphene layer number and modulating length on the performance are evaluated. It can be seen that the 3-dB bandwidths are all around 48 GHz for different cases of layer numbers and modulating lengths. The driving voltage and power consumption decreases with the increment of graphene layer number and graphene modulation length in the price of the optical loss. The six-layer graphene modulator presents a low-power consumption of 14 fJ/bit when L_g is 240 μm . The optimized modulator parameters are to be determined compromisingly based on presented rules.

References

- [1] Janner D, Lucchi F and Belmonte M 2007 *Opt. Express* **15** 10739
- [2] Pérez-Galacho D, Marris-Morini D and Stoffer R 2016 *Opt. Express* **24** 26332
- [3] Krishnamoorthy A V, Luff B J and Bijlani B 2012 *Opt. Express* **20** 22224
- [4] Sun X, Zhou L and Li X 2011 *Appl. Opt.* **50** 3428
- [5] Xiu C L, Shan W H and Xin J C 2019 *Acta Phys. Sin.* **68** 168102 (in Chinese)
- [6] Mo J W, Qiu Y W and Yi R B 2019 *Acta Phys. Sin.* **68** 156501 (in Chinese)
- [7] Wu C C, Guo X D and Hu H 2019 *Acta Phys. Sin.* **68** 148103 (in Chinese)
- [8] Koziol Z, Gawlik G and Jagielski J 2019 *Chin. Phys. B* **28** 096101
- [9] Li M, Qu G F and Wang Y Z 2019 *Chin. Phys. B* **28** 093401
- [10] Zhang X F, Liu Z H and Liu W L 2019 *Chin. Phys. B* **28** 086103
- [11] Fan C, Tian Y and Ren P 2019 *Chin. Phys. B* **28** 076105
- [12] Sun Z, Hasan T and Torrisi F 2010 *ACS Nano* **4** 803

- [13] Avouris P and Freitag M 2014 *IEEE J. Sel. Top. Quantum Electron.* **20** 6000112
- [14] Shi K, Zhao W and Lu Z 2013 *Opt. Lett.* **38** 4342
- [15] Xie C, Wang Y and Zhang Z X 2018 *Nano Today* **19** 41
- [16] Wu Z and Xu Y 2018 *Appl. Opt.* **57** 3260
- [17] Ye S W, Yuan F and Zou X H 2017 *IEEE J. Sel. Top. Quantum Electron.* **23** 3400105
- [18] Liu M, Yin X and Ulin-Avila E 2011 *Nature* **474** 64
- [19] Yang L, Hu T and Hao R 2013 *Opt. Lett.* **38** 2512
- [20] Liu M, Yin X and Zhang X 2012 *Nano. Lett.* **12** 1482
- [21] Hu Y, Pantouvaki M and Campenhout J 2016 *Laser Photon. Rev.* **10** 307
- [22] Mohsin M, Schall D and Otto M 2014 *Opt. Express* **22** 15292
- [23] Ji L, Zhang D and Xu Y 2013 *IEEE Photon. J.* **11** 7800911
- [24] Phatak A, Qin C and Goda K 2016 *Opt. Lett.* **41** 2501
- [25] Gosciniak J and Tan D T 2013 *Nanotechnology* **24** 185202
- [26] Mohsin M, Neumaier D and Schall D 2015 *Sci. Rep.* **5** 10967
- [27] Rodriguez S B, Yan R and Kelly M 2012 *Nat. Commun.* **3** 780
- [28] Phare C T, Y H Daniel Lee and Cardenas J 2015 *Nat. Photon.* **9** 511
- [29] Fan M, Yang H and Zheng P 2017 *Opt. Express* **25** 21619
- [30] Zhang X, Zhang Y B and Xiong C 2016 *J. Opt.* **18** 074016
- [31] Feng J and Akimoto R 2014 *IEEE Photon. Tech. Lett.* **26** 706
- [32] Bauters J F, Heck M J R and John D D 2011 *Opt. Express* **19** 24090
- [33] Shriramin L A and Thourhout D V 2017 *IEEE J. Sel. Top. Quantum Electron.* **23** 3600107
- [34] Wang J, Cheng Z and Shu C 2015 *IEEE Photon. Tech. Lett.* **27** 1765
- [35] Sorianello V, Midrio M and Romagnoli M 2015 *Opt. Express* **23** 6478
- [36] Hu X, Zhang Y and Chen D 2019 *J. Lightwave Technol.* **37** 2284
- [37] Zhong H, Zhang Z and Chen B 2015 *Nano Res.* **8** 1669
- [38] Bao Q and Loh K P 2012 *ACS Nano* **6** 3677
- [39] Stauber T, Peres N M R and Geim A K 2008 *Phys. Rev. B* **78** 085432
- [40] Wülbern J H, Hampe J and Petrov A 2009 *Appl. Phys. Lett.* **94** 241107
- [41] Ji L, Gao Y and Xu Y 2018 *IEEE J. Quantum Electron.* **54** 5200107
- [42] Yan J, Zhang Y and Kim P 2007 *Phys. Rev. Lett.* **98** 166802
- [43] Wang F, Zhang Y and Tian C 2008 *Science* **320** 206
- [44] Hwang C, Siegel D A and Mo S K 2012 *Sci. Rep.* **2** 590
- [45] Xu C, Jin Y and Yang L 2012 *Opt. Express* **20** 22398
- [46] Koester S J and Li M 2012 *Appl. Phys. Lett.* **100** 171107
- [47] Hu Y, Xiao X and Xu H 2012 *Opt. Express* **20** 15079
- [48] Cheng Z, Chen X and Wong C Y 2012 *Opt. Lett.* **37** 1217
- [49] Politi A, Cryan M J and Rarity J G 2008 *Science* **320** 646
- [50] Zhu X, Shi L and Schmidt M 2013 *Nano Lett.* **13** 4690
- [51] Zhu X, Yan W and Jepsen P U 2013 *Appl. Phys. Lett.* **102** 131101
- [52] Ding Y, Guan X and Zhu X 2017 *Nanoscale* **9** 15576